JOURNAL OF
Materials
CHEMISTRY

Structure and growth characteristics of $BaZrO_3$ films produced using an electrostatic assisted aerosol–gel deposition method

B. Su and K. L. Choy*

Department of Materials, Imperial College of Science, Technology and Medicine, Prince Consort Road, London, UK SW7 2BP. E-mail: k.choy@ic.ac.uk

Received 12th January 1999, Accepted 23rd April 1999

$BaZrO_3$ films have been fabricated using an electrostatic assisted aerosol–gel deposition (EAAD) method. The precursor was synthesised by reacting barium with 2-methoxyethanol and then mixed with zirconium *n*-propoxide in 2-methoxyethanol solvent. The aerosol was generated by electrostatic atomisation. The results showed that the aerosol was an oxo–alkoxide complex which transformed to $BaZrO_3$ at temperatures above 800 °C with some $BaCO_3$ formed as an intermediate product. Amorphous aerosol–gel films were deposited at an optimum temperature of 400 °C. Crystalline $BaZrO_3$ films could be produced by repeating the deposition and heat-treatment at 800 °C.

Introduction

Barium zirconate ($BaZrO_3$) is a technically important material owing to its excellent chemical and electrical properties. One of its important applications is in the production of high-quality high T_c superconducting materials.[1] $BaZrO_3$ has a cubic perovskite structure and a high theoretical density of 6.242 g cm^{-3}. It has a high melting point of *ca.* 2600 °C, and most importantly, shows no crystallographic phase transitions or chemical interactions with superconducting materials (*e.g.* $YBa_2Cu_3O_{7-\delta}$, YBCO) in the high temperature region of high T_c superconductor processing. Therefore, it is the ideal container material for the solution growth of single crystals of YBCO[2] and substrate or buffer layer for YBCO superconductors.[3] However, owing to the poor sinterability of $BaZrO_3$ powders, the fabrication of high-density bulk $BaZrO_3$ materials is very difficult and costly.[4] Another problem is that the materials made from sintered $BaZrO_3$ ceramics with high densities are very fragile and prone to cracks. An alternative process is to apply $BaZrO_3$ coatings or films on the substrate. More recently, $BaZrO_3$ coatings have shown another promising application as diffusion barriers in Bi(2223) multi-filamentary tapes to reduce ac losses due to interfilamentary coupling.[5] Few studies have been reported for the manufacture of $BaZrO_3$ films or coatings. $BaZrO_3$ thin films have been fabricated using sol–gel[6] and hydrothermal synthesis[7] methods. However, the film thickness is limited to only *ca.* 100–300 nm. Preparation of thick $BaZrO_3$ films or coatings have also been attempted recently using reactive liquid phase sintering and plasma spraying[8] and polymer painting.[9] However, neither of these methods was successful and the film properties need further improvement.

Here, we demonstrate the use of a novel and cost-effective film deposition technique, denoted electrostatic assisted aerosol–gel deposition (EAAD) for the fabrication of thick $BaZrO_3$ films (*e.g.* 10 μm). EAAD is a process which involves spraying atomised droplets across an electric field, where the droplets undergo gelation and/or decomposition near the vicinity of the heated substrate to form a layer of solid film. The relationship between film deposition conditions and microstructures will be discussed.

Experimental

The precursor solution for the deposition of $BaZrO_3$ was prepared as described in ref. 6. Barium metal (Aldrich, 99%) was allowed to react with 2-methoxyethanol (Aldrich, 99.9%) at room temperature and after the barium metal had dissolved completely, a stoichiometric amount of zirconium *n*-propoxide (Aldrich, 70 wt% solution in *n*-propanol) was added to the barium methoxyethoxide solution and refluxed/distilled at the boiling point of 2-methoxyethanol (124 °C) for 5 h. Then the final volume of yellow solution was adjusted using 2-methoxyethanol to obtain a 0.2 M precursor solution. All the chemicals were used without further purification.

The apparatus used for the film deposition has been described in ref. 10. An upward capillary-plate configuration was used to atomise and deliver the liquid precursor to a heated substrate under a high voltage (*e.g.* 10 kV) electric field. The substrate was a silver tape and the deposition area was *ca.* 12 cm^2. The deposition temperature was varied from 250 to 500 °C. Post-treatment was carried out in a tube furnace in air at 800 °C for 2 h.

The study of the decomposition of precursor was performed using a simultaneous TG–DTA apparatus (Stanton Redcroft STA-780) in a flowing air or argon atmosphere (60 ml min^{-1}) at a heating rate of 10 °C min^{-1}. The sample mass used in TG–DTA measurement was 15 mg. The microstructure evolution of the precursor during thermolysis was investigated by FTIR using a MIDAC M series FTIR spectrometer *via* transmission mode. Samples were prepared by mixing the precursor or pyrolysed precursor with KBr in a weight ratio of 1 : 9 using a mortar and pestle, and pressed into a pellet. Pure $BaZrO_3$ powder was used as a reference. The surface morphology and cross-section of the deposited films were characterised using scanning electron microscopy (SEM) (JEOL 220). The Ba/Zr ratio was measured using a Link 5082 energy dispersive X-ray (EDX) analysis attachment. The crystallinity of the films was characterised by X-ray diffraction (XRD) (Philips PW 1710) employing nickel-filtered monochromatic Cu-Kα radiation at 40 kV and 40 mA in steps of 0.05° 2θ and count times of 1 s $step^{-1}$.

Results

TG–DTA

Fig. 1 shows the TG–DTA curves of the precursor gel after evaporation of the solvent. It is clear that there are three stages involved during the thermal decomposition of the precursor. The first stage occurs at *ca.* 100 °C; a large endothermic peak is accompanied with *ca.* 8–10% weight loss. This is probably due to the evaporation of residual solvent in the

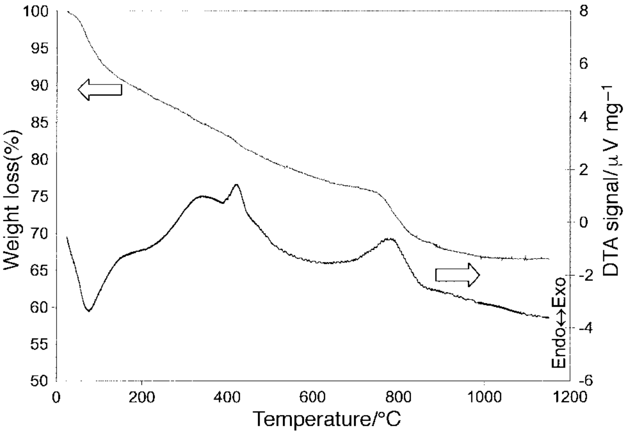

Fig. 1 TG–DTA curve of the precursor used for the deposition of $BaZrO_3$ films. The measurement was carried out in a flowing air atmosphere (60 ml min^{-1}).

gel. The second stage is around 400 °C, the endo-exothermal peaks are associated with the decomposition of organic groups in the precursor.[11] The weight loss (*ca.* 15%) is slow and gradual and occurs over a temperature range of 200–700 °C, indicating that the decomposition of the precursor to the final $BaZrO_3$ oxide is a complex and progressive process. A final weight loss (*ca.* 11%) associated with an exothermal peak is observed between 700 and 800 °C, which is due to the decomposition of barium carbonate into oxide as reported by Van Bael *et al.*[12] Similar weight loss behaviour was observed when the TG–DTA analysis was carried out under a flowing argon atmosphere, indicating that the formation of the intermediate barium carbonate product was from the initial precursor solution.

FTIR

Fig. 2 shows the FTIR curves of the precursor as a function of temperature. The most distinctive feature of the precursor solution is a broad absorption band around 3400 cm^{-1}, and bands at 1370 and 1585 cm^{-1}. The first band ($\nu_{O\text{–}H}$) is characteristic of O–H stretching of alcohol and adsorbed water, while the second double band feature is probably due to the symmetric and asymmetric stretching vibrations of carboxylate ion (CO_3^{2-}) arising from air contact.[13] At 200 °C, the free 2-methoxyethanol and water band at 3400 cm^{-1} disappears, while a shoulder band at 1450 cm^{-1} is now present. This band, along with other two sharp bands at 860 and 690 cm^{-1}, are characteristic features of $BaCO_3$,[11] which increase as the temperature is increased from 400–600 °C. At 800 °C, two broad bands at 1450 and 565 cm^{-1} are observed, with the latter attributed to the metal–oxide vibration of $BaZrO_3$. When the temperature is increased to 1000 °C or to 800 °C for a prolonged time (5 h), only vibration bands from $BaZrO_3$

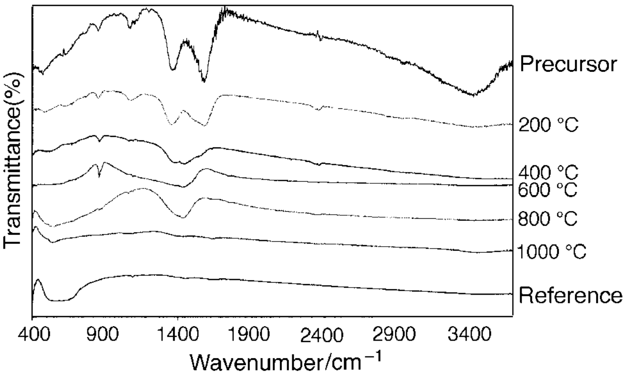

Fig. 2 FTIR spectra of the precursor as a function of temperature.

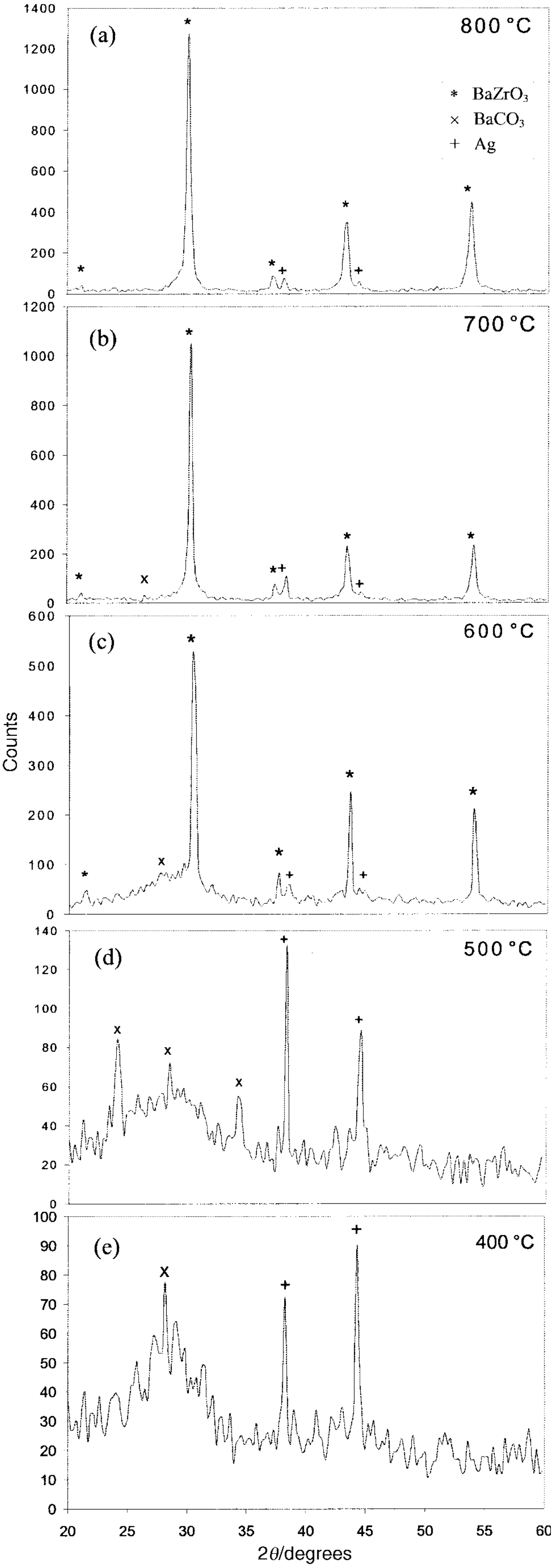

Fig. 3 XRD patterns of the films deposited at different temperatures.

are present as seen by comparison with a pure $BaZrO_3$ reference. This indicates that pure $BaZrO_3$ can be formed under our experimental conditions, in accord with the TG–DTA results.

XRD

Fig. 3 shows the XRD patterns of films deposited at different temperatures. At 400 °C, the first intermediate phase was identified as $BaCO_3$, which increased with increasing deposition temperature up to 600 °C. At 600 °C, crystalline $BaZrO_3$ was formed as a consequence of decomposition of organic groups of the precursor as revealed by the TG–DTA data. However, $BaCO_3$ was still present according to XRD until the temperature reached 800 °C, at which point only pure $BaZrO_3$ was present. These results were consistent with the above TG–DTA and FTIR results.

SEM

Fig. 4 shows SEM micrographs of the films deposited onto silver tapes at different temperatures. It can be seen that the deposition temperature range leading to the formation of smooth adherent films is very narrow. Crack-free films could be deposited at 400 °C. Below 380 °C, films with large cracks were formed whilst above 420 °C, porous and powdery films were formed. Thus optimum deposition temperature appears to be *ca.* 400 °C, where gelation and decomposition take place simultaneously leading to continuous crack-free films. The cross-section of the films showed that the films were uniform across the deposition area with thickness of *ca.* 10–15 µm.

It should be pointed out that the films deposited at 400 °C were amorphous and contained only a small amount of microcrystalline $BaCO_3$ phase as shown by XRD [Fig. 3(e)]. Further heat treatment was required to produce single-phase $BaZrO_3$ films. EDX analysis confirmed that the films were stoichoimetric with a Ba/Zr ratio of 1. During high temperature treatment, cracking may occur owing to further decomposition and transformation, especially for thick films. Multiple deposition/heat-treatment is necessary to minimise cracking of the films. Fig. 5 shows a $BaZrO_3$ film deposited on a silver tape *via* a multiple deposition/firing process.

Discussion

Structural evolution

In principle, the reaction of Ba metal with 2-methoxyethanol occurs are given by eqn. (1)

$$\mathrm{Ba\ (s) + 2MeOCH_2CH_2OH\ (l) \rightarrow Ba(OCH_2CH_2OMe)_2\ (l) + H_2(g)} \qquad (1)$$

However, a single-crystal X-ray study[14] showed that the actual product was an oxo–alkoxide $H_4Ba_6(\mu_6\text{-}O)(OCH_2CH_2OMe)_{14}$ which is composed of a central octahedral $Ba_6(\mu_6\text{-}O)$ unit supported by eight $\mu_3\text{–}\eta^2\text{-}OCH_2CH_2OMe$, four $\eta^2\text{–}OCH_2CH_2OMe$ and two $\eta^1\text{–}OCH_2CH_2OMe$ groups and intermolecular bonds.[14]

Zirconium *n*-propoxide reacts with the 2-methoxyethanol to give methoxyethoxide ligands [eqn. (2)].

$$\mathrm{Zr(OPr^n)_4\ (l) + 4MeOCH_2CH_2OH\ (l) \rightarrow Zr(OCH_2CH_2OMe)_4\ (l) + 4\ Pr^nOH\ (l)} \qquad (2)$$

Again, a recent study[15] has shown that Zr alkoxides contain admixtures of oxo-complexes such as $Zr_3O(OR)_{10}$ and $Zr_4O(OR)_{14}$. An oxo–alkoxide of composition $BaZrO(OR)_4{\cdot}n\mathrm{ROH}$ is reportedly formed in an equimolar alcoholic solution of Ba and Zr alkoxides.[16]

The origin of oxo–alkoxide formation is not very clear[17] although several explanations have been proposed. One such is an uncontrolled microhydrolysis reaction. However, in some cases, even under strictly controlled synthesis conditions, oxo–alkoxides are still formed. The following sequence of transformations [eqn. (3)] is proposed to take place on storage:[15]

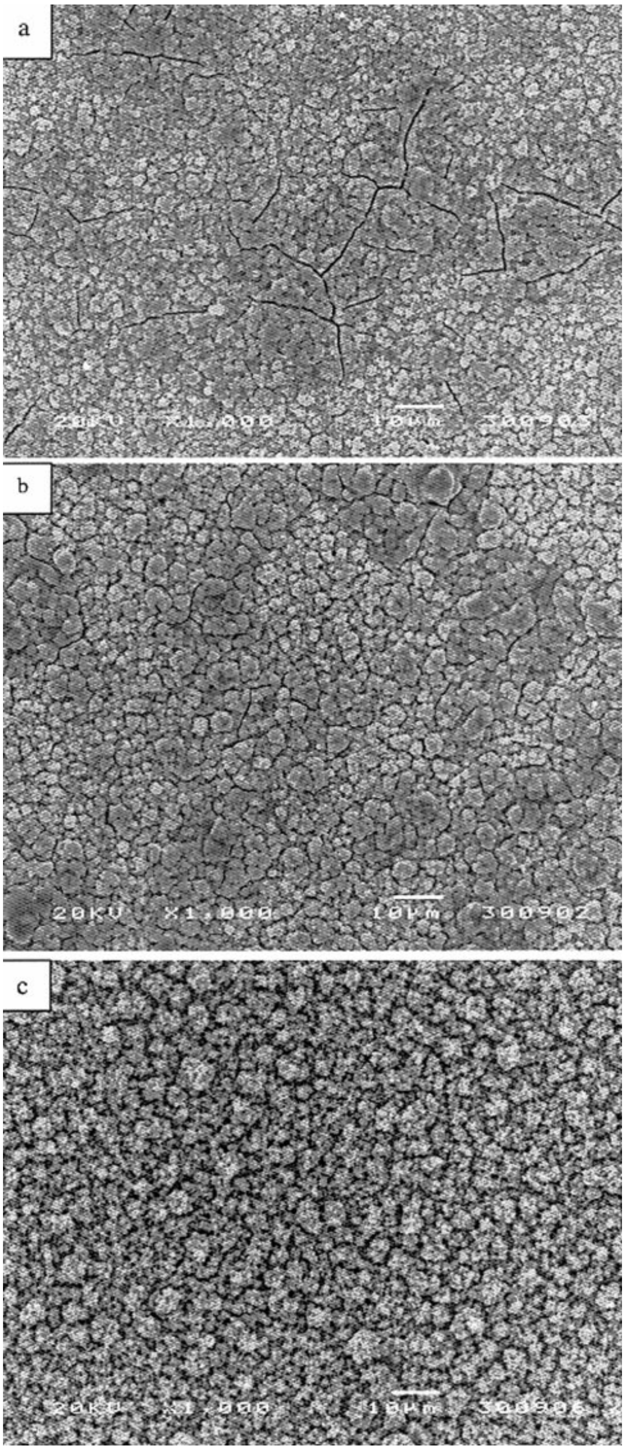

Fig. 4 SEM micrographs of the surface morphology of films deposited at (a) 380 °C; (b) 400 °C and (c) 420 °C. The film thickness is *ca.* 10 µm.

$$\mathrm{M(OR)}_n \xrightarrow[-\mathrm{R_2O}]{} \mathrm{MO(OR)}_{n-2} \xrightarrow[-\mathrm{R_2O}]{} \mathrm{MO_2(OR)_2} \qquad (3)$$

This reaction is accelerated by traces of moisture, heating and especially the presence of alkali or alkaline earth alkoxides. The appearance of oxo-groups in alkali and alkaline earth metal alkoxides can be caused by uncontrolled oxidation (*e.g.* by traces of oxygen dissolved in solvents used or present in the atmosphere). The primary products of oxidation contain

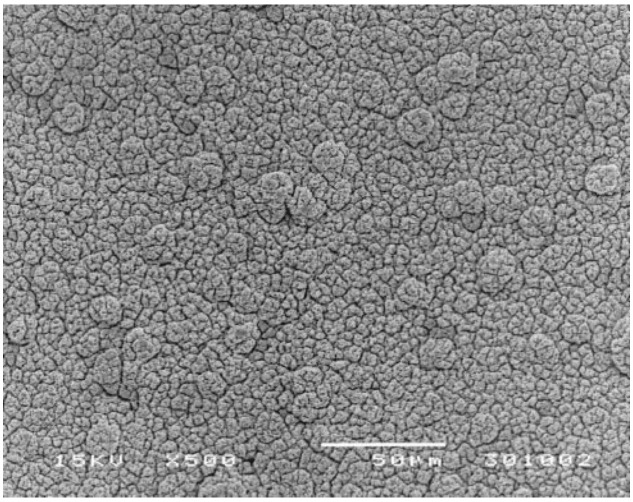

Fig. 5 Surface morphology of a $BaZrO_3$ film deposited at 400 °C and subsequently heat-treated at 800 °C for three cycles. The film thickness is *ca.* 20 µm.

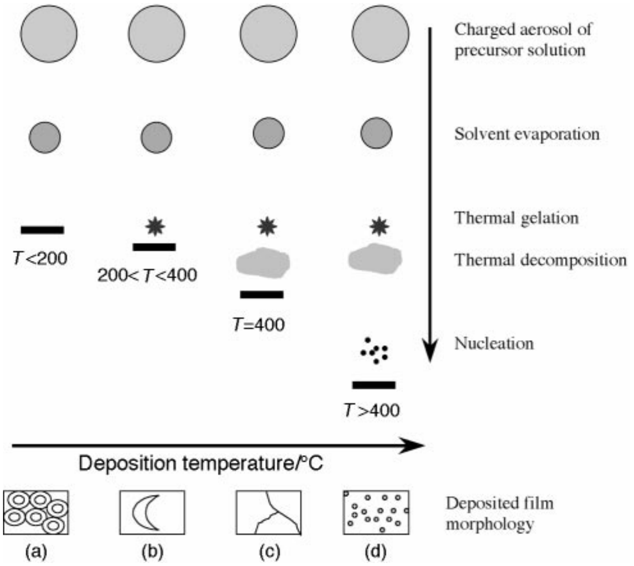

Fig. 6 A schematic diagram of the mechanism of film formation and morphology as a function of deposition temperature.

–OOR and –OOH groups,[18] which undergo radical decomposition to produce water, and gives rise to oxo- and HCO_2-groups in the structure of the precursors. Such reactions can take place only for the most ionic alkoxides, for which dissociation in solution is accompanied by liberation of OR^- anions, which can react with O_2. 2-Methoxyethoxides demonstrate the most pronounced trend towards oxidation.[15]

Therefore, the structure of precursor used for the deposition of $BaZrO_3$ films described here could be envisaged as an oxo–alkoxide complex, comprised of a BaZrO core surrounded by several $(OR)_m$ and $(ROH)_n$ ligands and carboxylate ion CO_3^{2-} arising from exposure to air. During thermal decomposition, the ROH ligands are evolved first (<200 °C) as indicated by the TG–DTA and FTIR results, followed by the decomposition of OR ligands (>350 °C) to form amorphous $BaZrO_3$. During this stage, $BaCO_3$ was formed as an intermediate product as revealed by FTIR and XRD results. When the temperature was increased to 600 °C, the decomposition is almost complete, resulting in the formation of crystalline $BaZrO_3$ along with a small amount of $BaCO_3$. Finally, when the temperature is increased to 800 °C, decomposition of $BaCO_3$ takes place and only single–phase $BaZrO_3$ is present in the film.

Morphology development

As can be seen from Fig. 4, the substrate temperature has a substantial influence on the surface morphology of the films deposited *via* the EAAD processing route. When the substrate temperature was too low (*e.g.* ⩽380 °C) or too high (*e.g.* ⩾420 °C), either films with large cracks or powders were formed. Fig. 6 shows a schematic diagram of the relationship between the deposition temperature and the film characteristics. Below 200 °C, charged aerosol droplets hit the substrate because the temperature is too low to vaporise the solvent in the droplets during migration to the substrate. Consequently a precipitate is formed after solvent evaporation [Fig. 6(a)]. When the temperature is increased, solvent evaporation and thermal gelation occurs during the aerosol transport, and a 'wet' film is formed with large cracks owing to rapid shrinkage of the film during aerosol–gel transformation as shown in Fig. 4(a) and 6(b). When the substrate temperature is increased to *ca.* 400 °C, the solvent is almost vaporised before hitting the substrate; thermal gelation and decomposition occur simultaneously on the substrate resulting in the deposition of crack-free films [Fig. 4(b) and 6(c)]. The optimum substrate temperature range is rather narrow. When the temperature is increased beyond 400 °C, solid particles are formed during transport of aerosol droplets to the substrate. The droplets dry up completely before reaching the substrate and porous films are formed as they hit the substrate [Fig. 4(c) and 6(d)]. Further increase in temperature leads to complete vaporisation and the precursor decomposes to form a vapour phase near the vicinity of the substrate and a heterogeneous chemical vapour deposition process is expected to occur.[19] However, since the decomposition of the precursor is a gradual process as shown by the TG–DTA results, both heterogeneous and homogeneous reactions may take place during the high temperature deposition. Therefore, a powdery film will be formed at higher temperatures (>400 °C). Crack-free films are obtained at *ca.* 400 °C, however they are mainly amorphous with only a small amount of microcrystalline $BaCO_3$ according to XRD. Further heat treatment is required to produce thick single-phase $BaZrO_3$ films.

Conclusions

$BaZrO_3$ films have been fabricated on silver tapes *via* a cost-effective electrostatic assisted aerosol–gel deposition (EAAD) technique. The precursor for the deposition of $BaZrO_3$ was synthesised *via* the alkoxide sol–gel route. The structure of the precursor is of an oxo–alkoxide complex. During deposition, $BaCO_3$ was observed as an intermediate product. Single-phase $BaZrO_3$ films were formed at temperatures above 800 °C. Repeated deposition/firing was required to produce thick crack-free and crystalline $BaZrO_3$ films. The surface morphology of the films was influenced by the substrate temperature which determined the deposition mechanism. The optimum temperature was found to be *ca.* 400 °C where aerosol gelation and decomposition occurred simultaneously.

Acknowledgements

The authors wish to thank EPSRC-ROPA (GR/L73562) for financial support.

References

1 A. Erb, T. Traulsen and G. Muller-Vogt, *J. Cryst. Growth*, 1994, **137**, 385.
2 A. Erb, E. Walker and R. Flukiger, *Physica C*, 1996, **258**, 9.
3 R. X. Liang, D. A. Bonn and W. N. Hardy, *Physica C*, 1998, **304**, 105.

4 N. M. Alford, A. Templeton and S. J. Penn, *Supercond. Sci. Technol.*, 1998, **11**, 703.
5 Y. B. Huang and R. Flukiger, *Physica C*, 1998, **294**, 71.
6 M. Paranthaman, S. S. Shoup, D. B. Beach, R. K. Williams and E. D. Specht, *Mater. Res. Bull.*, 1997, **32**, 1697.
7 V. M. Fuenzalida and M. E. Pilleux, *J. Mater. Res.*, 1995, **10**, 2749.
8 J. C. Schmidt, A. Tigges and G. J. Schmitz, *Mater. Sci. Eng. B*, 1998, **53**, 115.
9 J. Shi, J. E. Berger and X. S. Ling, *Physica C*, 1998, **301**, 215.
10 K. L. Choy, *Mater. World*, 1998, **6**, 144.
11 G. K. Chuah, S. Jaenicke, K. S. Chan, S. T. Khor and J. O. Hill, *J. Therm. Anal.*, 1993, **40**, 1157.
12 M. K. Van Bael, J. Mullens, R. Nouwen, J. Yperman and L. C. Van Poucke, *J. Therm. Anal.*, 1997, **48**, 989.
13 G. Busca, V. Buscaglia, M. Leoni and P. Nanni, *Chem. Mater.*, 1994, **6**, 955.
14 K. G. Caulton, M. H. Chisholm, S. R. Drake and J. C. Huffman, *J. Chem. Soc., Chem. Commun.*, 1990, 1498.
15 N. Ya. Turova, E. P. Turevskaya, M. I. Yanovskaya, A. I. Yanovsky, V. G. Kessler and D. E. Tcheboukov, *Polyhedron*, 1998, **17**, 899.
16 E. P. Turevskaya, D. V. Berdyev and N. Ya. Turova, *J. Sol–Gel Sci. Technol.*, 1997, **8**, 111.
17 N. Ya. Turova, *et al.*, *Polyhedron*, 1998, **17**, 899.
18 A. Le Berre, *Bull. Soc. Chim. Fr.*, 1961, **1198**, 1543.
19 G. Blandenet, M. Court and Y. Lagarde, *Thin Solid Films*, 1981, **77**, 81.

Paper 9/00342H